Journal of Hydroscience and Hydraulic Engineering
Vol. 18, No.1 May, 2000, 141-151

BEHAVIOR OF BED-MATERIAL PARTICLES AS A GRANULAR MATERIAL IN A BED-LOAD TRANSPORT PROCESS

By

Hitoshi GOTOH

Associate Professor, Department of Civil Engineering, Kyoto University,
Yoshida Hon-machi, Sakyo-ku, Kyoto, 606-8501, Japan,
e-mail: gotoh@coast.kuciv.kyoto-u.ac.jp

and

Tetsuo SAKAI

Professor, Department of Civil Engineering, Kyoto University,
e-mail: sakai@coast.kuciv.kyoto-u.ac.jp

ABSTRACT

Lagrangian simulation of sediment-particle motion is one of the most effective tools for the investigation of sediment transport mechanics. In the previous studies of Lagrangian simulation, the motion of sediment particle was traced on the fixed bed with protrusions, or the irregularly arranged bed-material particles. In this study, the behavior of the bed-material particles is simulated based on the Distinct Element Method, or DEM, to describe the detailed mechanism of the inter-particle momentum transfer. The velocity profile of the sediment particle and the existing probability, or concentration, of the sediment particle are estimated on the basis of the simulation data of the particle's trajectory. Other kinds of fundamental characteristics of the sediment transport, such as the thickness of the sediment moving layer and the sediment transport rate are also estimated.

INTRODUCTION

To explain the non-equilibrium sediment transport process, the irregularity of the sediment-particle motion is the key factor. Lagrangian simulation of sediment motion, which can simulate the detailed motion of sediment particle, is the most effective tool to describe the irregular motion of sediment particle. The most of the previous Lagrangian simulation have focused on the bed-load particles and the suspended particles accelerated by the high-velocity water-flow; while the behavior of the bed-material particles, which interact with the actively-moving particles, have never been treated directly. In other words, the most of the previous studies have treated the bed-material particles as the fixed rough bed, hence the interaction between the actively-moving particles and bed-material particles has not been treated explicitly. Specifically speaking, the effect of the slight motion of bed-material particles due to the collision with actively-moving particles was taken into account through the coefficient of restitution in the inelastic collision model, in which the hypothetical repulsing plane, or a fixed wall, was supposed between the bed-material particles and the actively moving particles. The coefficient of restitution was tuned by considering the agreement between the simulated characteristics and the experimental data of the sediment transport rate, or the thickness of sediment moving layer.

The simplification of the previous Lagrangian simulations of sediment motion primarily was caused by the deficiency of the performance of computer in those days, because the Lagrangian simulation requires huge amount of iterating procedures for calculating all of the instantaneous interparticle collisions occurring frequently. Recently, the improvement of the computer performance and the development of the numerical tools for the analysis of the granular material provide us the sufficient circumstances for conducting the direct simulation of the motion of individual sediment particle by introducing the granular-material simulation. Mishima, Akiyama and Tsuchiya (1) conducted the numerical simulation of the collision of wind-driven sediment particle with movable bed by using the Distinct Element Method originally proposed by Cundall and Strack (2). Haff and Anderson (3) also analyzed the impact of the collision between the actively moving particle and the bed-material particles in an aerolian saltation.

Authors have analyzed the behavior of the surface sheared sand layer based on the DEM (Sakai and Gotoh (4) and Gotoh and Sakai (5)) . In these studies, the high-velocity-sheetflow motion of the sediment layer under the extremely high bottom-shear stress was investigated, therefore the slight numerical instability of the DEM, which is characteristics as the explicit numerical code, did not affect severely to the numerical solutions. Because the initial non-zero velocity of the particle, which should be ideally zero, due to the numerical instability of the DEM can be negligible in comparison with the velocity level of particles moving in the sheetflow.

In this study, the parameters of the DEM were tuned to keep the sufficient stability of sand layer without the action of the flow shear. Furthermore, to simulate the behavior of the surface-sheared-sand layer under the wide range of the bottom shear stress of the water flow, the effect of the turbulence was considered by simulating the irregular time series of the flow velocity with the random numbers generated by computer. Consequently, the behavior of the sand layer in various situations, such as the initiation of sediment motion, the bed-load motion represented by the saltation, the suspension, and the sheetflow motion, were simulated in this study.

SIMULATION MODEL

Governing equations

The sediment particles are modeled by the rigid cylinders with an uniform diameter. Among each cylinder, the spring and dashpot systems are introduced to express the particle/particle interaction. Equations of motion of the individual particle are solved by the explicit method in the vertically two-dimensional plane. In other words, the motion of spherical particles confined between two vertical walls, which keeps the same distance as the diameter of the particle, is numerically traced (see Gotoh and Sakai (5)).

Equations of motion of the i-th particle in the vertically two-dimensional coordinate are as follows:

$$\rho\left(\frac{\sigma}{\rho}+C_M\right)A_3 d^3\frac{\mathrm{d}u_{pi}}{\mathrm{d}t}=\sum_j\left\{-f_n\cos\alpha_{ij}+f_s\sin\alpha_{ij}\right\}_j + \frac{1}{2}\rho C_D\sqrt{\left(U+u-u_{pi}\right)^2+\left(v-v_{pi}\right)^2}\left(U+u-u_{pi}\right)A_2 d^2 \tag{1}$$

$$\rho\left(\frac{\sigma}{\rho}+C_M\right)A_3 d^3\frac{\mathrm{d}v_{pi}}{\mathrm{d}t}=\sum_j\left\{-f_n\sin\alpha_{ij}+f\cos\alpha_{ij}\right\}_j + \frac{1}{2}\rho C_D\sqrt{\left(U+u-u_{pi}\right)^2+\left(v-v_{pi}\right)^2}\left(v-v_{pi}\right)A_2 d^2-\rho\left(\frac{\sigma}{\rho}-1\right)A_3 d^3 g \tag{2}$$

$$\frac{\pi d^5}{32}\frac{\mathrm{d}\omega_{pi}}{\mathrm{d}t}=\frac{d}{2}\cdot\sum_j\left\{f_s\right\}_j \tag{3}$$

$$C_D=C_{D\infty}+\frac{24\nu}{|\mathbf{u}-\mathbf{u}_p|d} \tag{4}$$

in which x, y=streamwise and upward-vertical coordinates; ρ=density of fluid; σ=density of sediment particle; C_M=added-mass coefficient (C_M=0.5); A_2, A_3=two- and three-dimensional geometrical coefficients of sediment particle ($A_2=\pi/4$ and $A_3=\pi/6$ for the spherical particle); d=diameter of sediment particle; u_{pi}, v_{pi}=velocity of particles in x and y directions; f_n, f_s=normal and tangential components of the force acting on the contacting plane between the i-th and j-th particles on the local coordinate system n-s; α_{ij}=contacting angle between the i-th and j-th particles; C_D=drag coefficient ($C_{D\infty}$=0.4); U=mean velocity component in x direction; u, v=fluctuating velocity components in x and y directions; g=gravitational acceleration; and ω_{pi}=angular velocity of the i-th particle. These sets of the equation of motion are solved explicitly to trace the motion of the individual particles.

Inter-particle acting force

Between two contacting particles, springs and dashpots are assumed in both of the normal and tangential direction, to describe the dynamic interparticle relation. The acting force between the i-th and j-th particles in normal and tangential direction, f_n and f_s, can be written as follows:

$$f_n(t) = e_n(t) + d_n(t) \tag{5}$$

$$f_s(t) = e_s(t) + d_s(t) \tag{6}$$

$$e_n(t) = \min\{e_n(t-\Delta t) + k_n \cdot \Delta\xi_n,\ e_{nmax}\} \tag{7}$$

$$d_n(t) = \eta_n \cdot \Delta\dot{\xi}_n \tag{8}$$

$$e_s(t) = \min\{e_s(t-\Delta t) + k_s \cdot \Delta\xi_s,\ e_{smax}\} \tag{9}$$

$$d_s(t) = \eta_s \cdot \Delta\dot{\xi}_s \tag{10}$$

in which e_n, e_s=forces working on springs; d_n, d_s=forces working on dashpots; $\Delta\xi_n$, $\Delta\xi_s$=displacement of particle during the time Δt (Δt=time step of the calculation); k_n, k_s=spring constants; and η_n, η_s=damping coefficients. In nature, sediment motion is three-dimensional; while in this simulation, particles move in the vertically-two-dimensional plane. To compensate a gap between the model and the prototype, the effect of the aggregation of particles is simply expressed by introducing the upper limit of the compression force acting on the spring, e_{nmax}, e_{smax}.

In this simulation, particles are non-cohesive, hence the joint, which has no resistance to the tensile force, is assumed in the normal direction. While, in the tangential direction, the frictional force works. To describe this characteristics, the joint, which slips at the limit of the shear stress, is assumed in the tangential direction. These joints can be formulated as follows:

$$f_n(t) = f_s(t) = 0 \quad when \quad e_n(t) < 0 \tag{11}$$

$$f_s(t) = \mu \cdot \mathrm{SIGN}(e_n(t), e_s(t)) \quad when \quad |e_s(t)| > \mu \cdot e_n(t) \tag{12}$$

$$\mathrm{SIGN}(a,b) = \begin{cases} |a| & when \quad b \geq 0 \\ -|a| & when \quad b < 0 \end{cases} \tag{13}$$

in which μ=coefficient of friction.

Simulation of flow turbulence

The time series of the flow turbulence is simulated by the simple Monte Carlo method. The fluctuating velocity components of the flow can be written as follows:

$$u(t) = r_u \cdot \sqrt{\overline{u^2}} \quad ; \quad v(t) = r_v \cdot \sqrt{\overline{v^2}} \tag{14}$$

in which r_u, r_v=random numbers following to the standard Gauss distribution in x and y directions; and $\sqrt{\overline{u^2}}, \sqrt{\overline{v^2}}$ =turbulent intensities in x and y directions. The two series of random numbers satisfy the two-dimensional Gauss distribution as follows:

$$f_r(r_u, r_v) = \frac{1}{\sqrt{2\pi}} \exp\left(-\frac{r_u^2}{2}\right) \frac{1}{\sqrt{2\pi}\sqrt{1-\gamma^2}} \times \exp\left\{-\frac{(r_v - \gamma \cdot r_u)^2}{2(1-\gamma^2)}\right\} \tag{15}$$

in which γ=cross correlation coefficient of two series of the random numbers. Eq. 15 can be re-written through an simple variable transformation as follows:

$$r_u = \xi_r \quad ; \quad r_v = \gamma \cdot \xi_r + \sqrt{1-\gamma^2} \cdot \zeta_r \tag{16}$$

Turbulent intensities is given by the semi-empirical formulation by Nezu (6) as follows:

$$\frac{\sqrt{\overline{u^2}}}{u_*} = 2.30 \exp\left(-\frac{y}{h}\right) \quad ; \quad \frac{\sqrt{\overline{v^2}}}{u_*} = 1.27 \exp\left(-\frac{y}{h}\right) \tag{17}$$

in which h=water depth; and u_*=shear velocity. The cross-correlation coefficient of two turbulent velocity components can be related to the Reynolds stress as follows:

$$\gamma = \frac{-\overline{uv}}{\sqrt{\overline{u^2}}\sqrt{\overline{v^2}}} = 0.342\left(1-\frac{y}{h}\right)\Big/\exp\left(\frac{2y}{h}\right) \qquad (18)$$

Initial and boundary conditions

The calculating domain is schematically shown in Fig. 1. In this simulation, the streamwise uniform condition is treated, therefore, the both sides of the calculating domain are the periodic boundaries. The bottom boundary is the fixed rough bed constituted by the particles with the same diameter as the moving particles. The uniform diameter particles arranged regularly often lead to the hexagonal packing structure, that are difficult to be dilated by shearing. To avoid the hexagonal packing, the initial location of particles are slightly disturbed by generating random number in the packing calculation. During the packing process, the velocity of particles are monitored to assess the convergence of the packing calculation. The time for the packing is 0.1 s.

After the packing, the main calculation is performed to trace the motion of the sediment particles under the action of the shear force. In reality, the fluid force acting on particle has the very complicated mechanism, such as the interaction between two-approaching particles due to the viscosity of fluid between them, and the wake behind particles. In this paper, these microstructure of the fluid around particle are simplified, in order to focus on the particle-particle interaction, or the dominant mechanism of highly-concentrated particle flow.

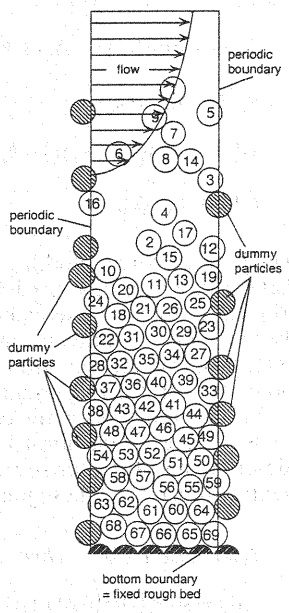

Fig. 1 Schematic expression of the calculating domain

The test particle is 0.5 cm in diameter and 2.65 in specific gravity. In the calculating domain, totally 69 particles are located in 15 layers: there are 5 particles in each layer except the surface layer, and 4 particles exist at the surface layer for the easy initiation of the particle's motion. The origin of the vertical coordinate is the averaged height of sand-surface constituting particles at the initial state of the calculation. The model constants are shown in Table 1. In this study, totally 5 cases of the calculation were executed for the different magnitude of the bottom shear stress. For all the cases, the water depth was 20 cm, then the bulk mean flow velocity was changed to set the different magnitude of the bottom shear.

CHARACTERISTICS OF INSTANTANEOUS PARTICLE MOTION

Figure 2 shows the snapshots of the motion of the particle. In the case of τ_*=0.05, the loose structure of the particles with a large porosity, the width of which is a few times as long as the diameter of particles, can be found in the neighborhood of the sand surface. In the case of τ_*=0.25, the bottom of the loose structure of the particles reaches to the level y/d=-5.0, and the moving layer of the particles becomes ten times as large as the diameter of particles. The moving layer of the particles increases with the bottom shear stress, τ_*. In the case of τ_*=3.0, some particle saltates higher than 20 times of particle diameter. While the loose structure of the particles develops gradually in downward direction with the increase of the bottom shear. In the case of τ_*=3.0, the bottom-wall neighboring particles stand still.

Table 1 Model constants

k_n	9.45×106 N/m
k_s	2.36×106 N/m
η_n	0.4 Ns/m
η_s	0.2 Ns/m
μ	0.5
e_{nmax}	7.5×102 N
e_{smax}	3.5 N
Δt	2.0×10-5 s

Figure 3 shows the typical particle trajectories for the different bottom shear stress, τ_*. The dashed lines in each figure shows the displayed area for the smaller-bottom-shear-stress cases. In the case of τ_*=0.05, the moving particle contacting frequently with the bottom surface can be found in the bottom neighboring region. The particle, the trajectory of which is shown by the thick line, is going down beneath the initial sand surface level, and then it stops after a few up-and-down motion. This shows the existence of the exchange between the moving particles and the bottom constituting particles. In the case of τ_*=0.25, the height of the moving layer increases, and then the saltation becomes clearly. In the case of τ_*=1.5 and 3.0,

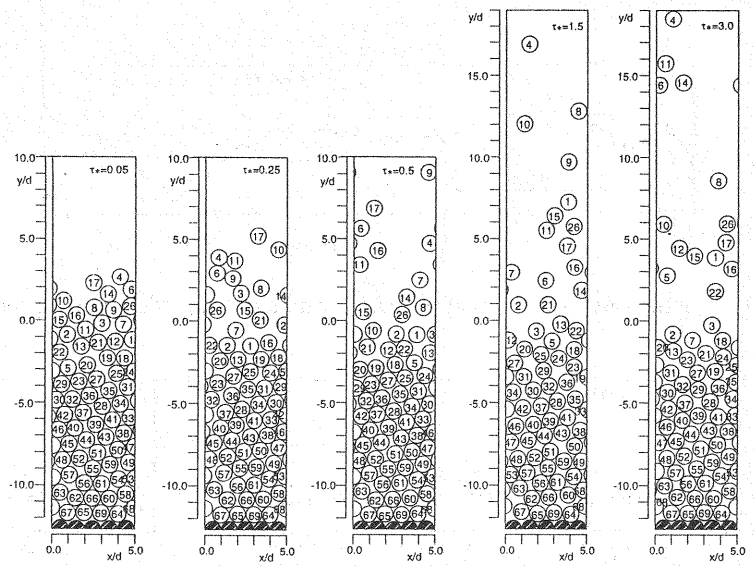

Fig. 2 Snapshots of the motion of particles

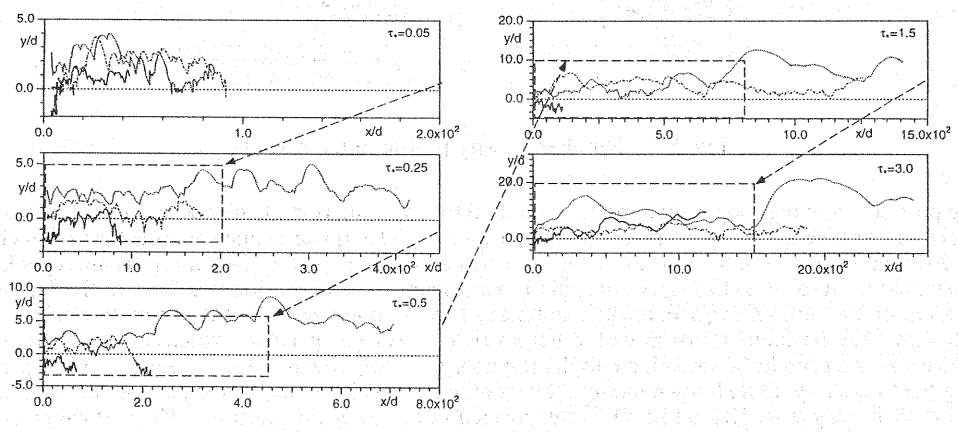

Fig. 3 Typical particle trajectories

the development of the moving layer of the particle becomes remarkably, consequently, some particles shows the water-depth-scale vertical motion. In these particles, some particles are moving up-and-down without contacting with the bottom surface, the trajectories of which is smoother than that of the particles with the frequent inter-particle collisions. These trajectories indicates the existence of the suspension.

AVERAGED STRUCTURE OF PARTICLE MOTION

Number density of particles

The trajectories of the moving particles indicated the coexistence of the different modes of sediment motion such as the saltation, the suspension and the sheetflow motion. To estimate the existing probability of each moving mode, all of the particle trajectories are classified on the basis of the following references.

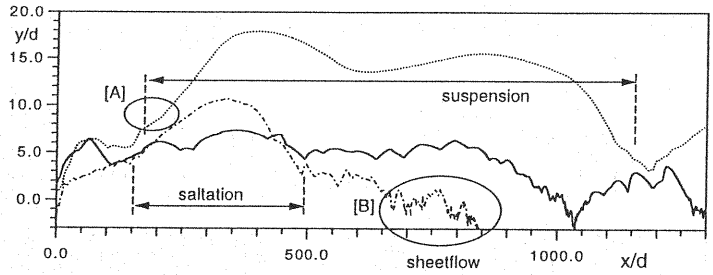

Fig. 4 Schematic expression of the classification of the particle moving mode

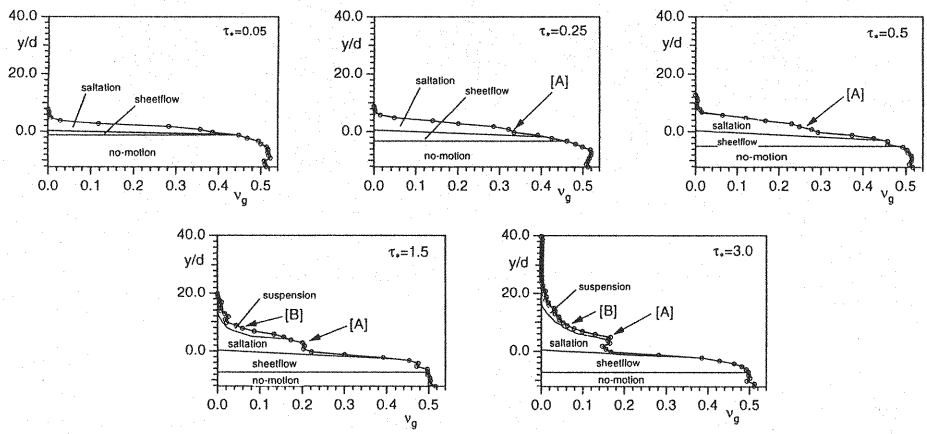

Fig. 5 Number-density profile of the particle

i) The particles moving longer then the few hundred times of the particle diameter without contacting with bottom surface are categorized as the suspension. ii) The upward concave trajectories, which are quite different from that of the typical saltations, (the part of the trajectory [A] in Fig. 4) are regarded as the transition form saltation to suspension. iii) The termination of suspension is defined as the deposition of particle on the bottom surface, or the existence of the frequently up-and-down motion of particle, which shows the frequent collision with other particles. iv) The particle, which does not satisfy the conditions i) or ii) and has a smooth parabolic trajectory, is categorized as the saltation. v) The particle having the frequently up-and-down motion, the amplitude of which is within the particle diameter scale, (the part of the trajectory [B] in Fig. 4) is categorized as the sheetflow motion. The vertical profile of the existing probability of each moving mode is calculated by measuring the length of trajectories in each layers with judging the moving mode based on the above references.

Figure 5 shows the number-density profile of moving particles, which is similar to the concentration profile of particles. The number density is constant in the deposition layer beneath y/d=-5.0, in witch the motion of the particle is inactive, and decreases drastically at the entrance of the moving layer. This characteristics are common to all the cases. In the case of τ_*=0.05, the number density simply decreases in the upward direction. In the cases of τ_*=0.25 and 0.5, in which the saltation is predominant, the gradient of the profile changes in the middle of the decreasing range (the part of the profile [A] in Fig. 5). This tendency is becoming to be clear with the increase of the bottom shear stress, τ_*. In the cases of τ_*=3.0, the clear peak of the profile (the part of the profile [A] in Fig. 5) is found. This peak was also found in the previous results of the numerical simulation of the saltation on a fixed bed (see Gotoh, Tsujimoto and Nakagawa (7)). On the movable bed, the elevation of the bed surface is uncertain in comparison with the fixed bed, hence the existence of the peak of the number-density profile also unclear on the movable bed.

In the cases of τ_*=1.5 and 3.0, the upward concave profile (the part of the profile [B] in Fig. 5) is

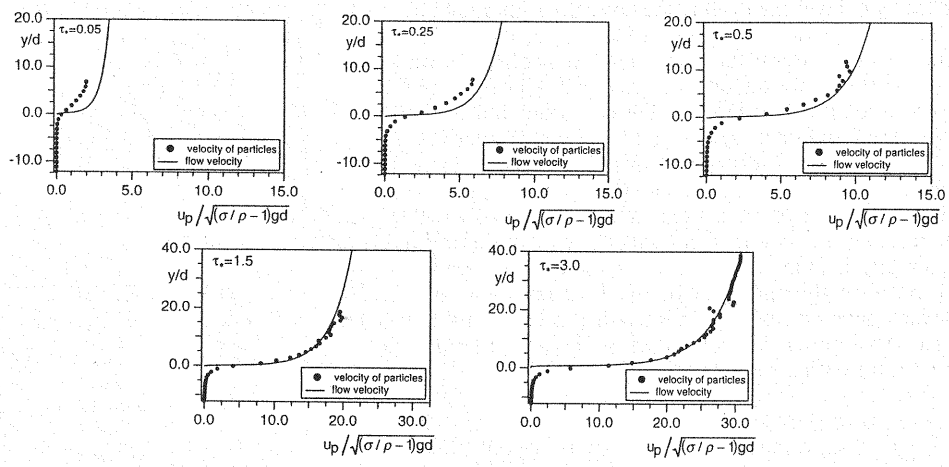

Fig. 6 Averaged velocity profile of the moving particles

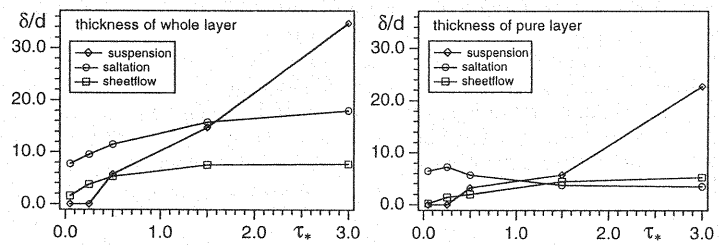

Fig. 7 Thickness of the moving layer

found at the upper edge of the number-density profile. This characteristic is similar to the negative exponential profile, which is the solution of the one-dimensional diffusion equation. The classification of the moving mode shows the existence of the suspension in this region, hence this upward concave profile indicates the contribution of the suspension.

Moving velocity of particles

Figure 6 shows the averaged velocity profiles of the moving particles. The mean velocity profiles of the fluid are also shown in these figures. In all the cases, there exist a non-zero region of the velocity of particle beneath the elevation, at which the flow velocity becomes zero. This non-zero region of particle velocity beneath the origin of flow velocity, which is about twice as thick as the particle diameter in the case of τ_*=0.05, increases with the bottom shear stress. It almost has completed the developing process with having the thickness about 5 times as the particle diameter in the case of τ_*=0.25.

Looking at the region above y/d=0.0, the velocity difference between flow and particle decreases with the increase of the bottom shear stress. In principle, the decrease of the bottom-contacting frequency of the particle due to the development of the transition from saltation to suspension makes the velocity difference between flow and particle small. Consequently, the mean velocity difference between flow and particle can be negligible in the suspension. The behavior of the velocity profile calculated by the present model with the increase of the bottom shear stress shows the existence of the suspension under the high bottom shear.

Thickness of the particle moving layer

Figure 7 shows the change of the thickness of the saltation layer, the suspension layer, and the sheetflow layer with the bottom shear stress. There is an overlapping region of different moving modes, hence the two definition of the moving layer are employed. The whole layer means that the layer

includes the overlapping region with other moving modes, while the pure layer means that the layer does not includes the coexisting region of different moving modes. The thickness of the suspension layer and the sheetflow layer increase with the bottom shear stress for both of the two definitions of moving layer. On the other hand, the saltation-layer thickness shows a different characteristic. The whole layer thickness of the saltation shows the same tendencies with the suspension and the sheetflow, but the pure layer thickness of the saltation decrease gradually with the increase of the bottom shear with the exception of the small bottom shear region $\tau_*<0.25$. Although the saltation develops with the increase of the bottom shear, the downward development of the suspension layer and the upward development of the sheetflow layer apparently suppress the existing region of the saltation.

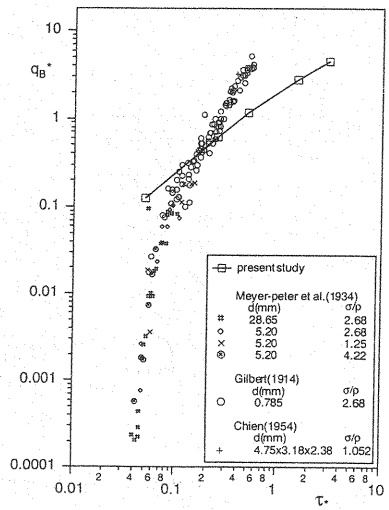

Fig. 8 Sediment transport rate

Sediment transport rate

Figure 8 shows the sediment transport rate calculated by integrating the product of the sediment moving velocity and the number density of the sediment estimated by the present model. Some experimental results are also shown in this figure. The agreement of present simulation with the experiments are good, although there is a discrepancy in detail. The present model gives the overestimation for the small bottom shear, and gives the underestimation for the large bottom shear. This tendensy can be interprited as follows. The present model is the one-way calculation, namely the calculation of the particle motion under the given condition of the flow velocity. Hence the origin of the flow velocity is fixed, in other words, the origin of the flow velocity does not descend with the decrease of the number density of particle due to the pick-up of the bottom constituting particles by the bottom shear. This assumption of the present model suppresses the development of the moving layer thickness, or the sediment transport rate. On the other hand, the loss of the fluid momentum to support the motion of the sediment particle is not taken into account, because the present model is the one-way model. Due to this assumption, the driving force of the sediment is rather overestimated. In the small bottom shear region, the downward shift of the origin of the flow velocity is negligible, hence the effect of the second assumption, or the error of the momentum loss of fluid, plays a major role. Consequently, the sediment transport rate is overestimated in the small bottom shear region.

FLUID-PARTICLE AND PARTICLE-PARTICLE INTERACTIONS

Fluid-particle interaction

Not only the interparticle collision but also the fluid-particle interaction play an important role, especially under the high sediment concentration. The present simulation, or the one-way method under the assumption of pure-water flow, provides the first order approximated solution of the drag force profile of the multiphase flow model for the flow-particle interaction. The characteristics of the drag force, or the interaction terms of the multiphase flow model, is examined for the preparation of the hybrid model of the DEM and the multiphase flow model.

Figure 9 shows the mean drag force profile in the case of $\tau_*=1.5$. The F_{dx} and F_{dy} mean the horizontal and vertical components of the mean drag force, respectively. The positive sign means that the particle is accelerated by the flow. The horizontal drag force is small in the region of $y/d>10.0$, in which the number density of the particle is small. And it increases drastically with moving downward. In the region, $0.0<y/d< 10.0$, the saltation is predominant, hence the saltating particles, which are decelerated by the energy loss of the collision at the bottom, are accelerated by the fluid. While, in the zero-fluid-velocity region, $y/d< 0.0$, the drag force acts on the particle in the direction to decelerate the particle.

The vertical component of the drag force has the value less than 10% of its horizontal component. In the region, $-1.0<y/d< 5.0$, in which the number density of the particle is large, the drag force act in the direction to promote the deposition of the particle, while in other region, the vertical drag force act in the direction to promote the upward motion of the particle. These characteristics of the vertical drag force plays an important role to entrain the sheetflow particles into saltation, to keep suspension in a long reach, and to promote the collision of saltating particles with the bottom.

Figure 10 shows the standard deviation profile of drag forces. The σ_{fdx} and σ_{fdy} mean the horizontal and vertical components of the standard deviation of drag force, respectively. In the region, $0.0<y/d<5.0$, in which the number density of the particle is large and the motion of the particle is active, the frequency of the interparticle collision is also large, consequently, the magnitude of the drag force fluctuation becomes large.

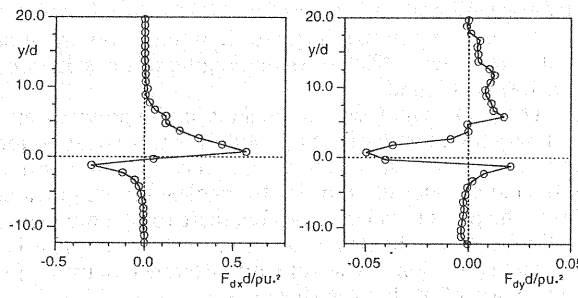

Fig. 9 Mean drag force profile

Interparticle Collision

Figure 11 shows the inter-particle-collision-frequency profile. The average of the moving length of particle during the two collisions is also shown in this figure. The frequency of the collision has a peak at the elevation $y/d\approx-3.0$, which belongs to the pure sheetflow region. This means that the sheetflow particles collide each other frequently. The collision-frequency distribution decrease with moving downward form the elevation at the peak, and it becomes zero at the elevation $y/d\approx-7.5$, which is the boundary of the sheetflow layer and the deposition layer. On the way of the decreasing region of the collision-frequency distribution with moving upward form the elevation at the peak, the rate of the decrease once becomes smaller at the elevation $0.0<y/d<4.0$ (the part of the profile [A] in Fig. 11). This region corresponds to the gradient-changing region of the particle-number density (the part of the profile [A] in Fig. 5). The collision-frequency profile becomes zero at the elevation $y/d=11.0$, which is the transition point from saltation to suspension. The average of the moving length of particle during the two collisions exponentially increases with moving upward from the elevation $y/d\approx5.0$, which is the beginning point of the existence of the suspension.

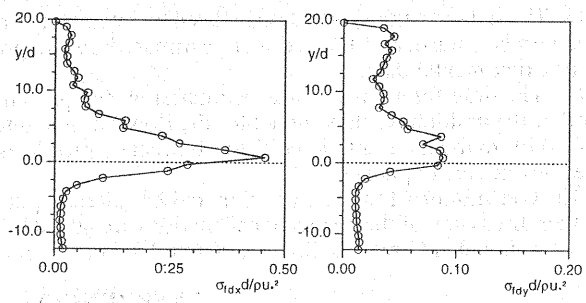

Fig. 10 Standard deviation profile of the drag force

CONCLUSIONS

In this study, the behavior of the surface sheared sand layer under the wide range of the bottom shear stress of the water flow was simulated based on the DEM with taking the irregular time series of the flow velocity into account by generating the random number. The behavior of the sand layer in various condition of the bottom-shear stress, such as the initiation of sediment motion, the bed-load motion represented by the saltation, the suspension, the sheetflow motion, and coexistence of these different moving modes were simulated in this study. The results obtained in this study are summarized below:

(1) Through the snapshots of particle motion, the typical instantaneous motion of the particles are shown.

(2) In some typical trajectories of the particle, the existence of the exchange between the moving particles and the bottom constituting particles can be found.

(3) The transition from the saltation to the

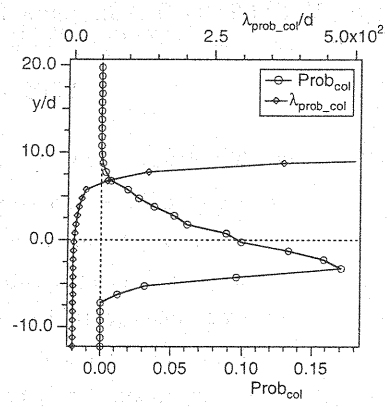

Fig. 11 Interparticle-collision frequency

suspension, and other kinds of the transition between two different moving mode can be found in the simulated trajectories.

(4) The existing probability profile of each moving mode was estimated by assessing all of the simulated trajectories. The coexisting region of the saltation and suspension, and that of the saltation and sheetflow was found.

(5) The peak, which was pointed out in the previous numerical simulation of the saltation on the fixed bed, was found under the high-bottom-shear-stress action in this study. On the movable bed, the elevation of the bed surface is uncertain in comparison with the fixed bed, hence the existence of the peak of the number-density profile also unclear on the movable bed.

(6) In the particle-velocity profile, there exist a non-zero region of the velocity of particle beneath the elevation, at which the flow velocity becomes zero. This is the result of the momentum transport due to interparticle collision. The velocity difference between flow and particle above y/d=0.0 decreases with the increase of the bottom shear stress.

(7) The whole layer thickness of the saltation, the suspension and the sheetflow increase with the bottom shear stress, but the pure layer thickness of the saltation decrease gradually with the increase of the bottom shear.

(8) The sediment transport rate calculated by integrating the product of the sediment moving velocity and the number density of the sediment estimated by the present model agrees fairly well with the pervious experimental data.

(9) The drag force profile was estimated by the present model as the first order approximated solution of the multiphase flow model for the flow-particle interaction.

(10) From the interparticle-collision-frequency profile estimated in this study, the characteristics of other profiles are explained.

The constitution of the numerical model has already published in Japanese (8), but it revised and the further discussion of the results of calculations are added herein. The authors express their gratitude to Mr. Atsushi Sakai (Graduate Student, Kyoto University) for his helps for numerical data processing.

REFERENCES

1. Mishima, M., Akiyama, S. and Tsuchiya, Y.: Numerical study of grain-bed impacts in blown sand, *Proc. Coastal Engrg., JSCE*, Vol. 40, pp. 271-275, 1993(in Japanese).
2. Cundall, P. A. and Strack, O. D. L.: A discrete numerical model for granular assembles, *Geothechnique* 29, No. 1,pp. 47-65, 1979.
3. Haff, P. K. and Anderson, R. S.: Grain scale simulation of loose sedimentary beds: The example of grain-bed impact in aeolian saltation, *Sedimentology*, Vol. 40, pp. 175-198, 1993.
4. Sakai, T. and Gotoh, H.: Numerical Simulation of Sediment Transport in Sheetflow Regime, *Proc. IAHR Congress*, London, UK, Vol. 3, pp. 299-304, 1995.
5. Gotoh, H. and Sakai, T.: Numerical Simulation of Sheetflow as Granular Material, *Jour. of Waterway, Port, Coastal, and Ocean Engrg., ASCE*, Vol. 123, No. 6, pp.329-336, 1997.
6. Nezu, I.: *Turbulent structure in open channel flows*, Ph. D Thesis presented to Kyoto University, Kyoto Japan, 1977(in Japanese).
7. Gotoh, H., Tsujimoto, T. and Nakagawa, H.: Numerical model of interphase momentum transfer and interparticle collision in bed-load layer, *Proc. APD-IAHR*, Singapore, pp.565-572, 1994.
8. Gotoh, H. and Sakai, T.: Interaction between transported-sediment particle and bed-material particles, *Proc. Hydraulic Eng., JSCE*, Vol. 41, pp. 819-824, 1997(in Japanese).

APPENDIX - NOTATION

The following symbols are used in this paper:

A_2, A_3 = two- and three-dimensional geometrical coefficients of sediment particle ($A_2=\pi/4$ and $A_3=\pi/6$ for the spherical particle);

C_D = drag coefficient ($C_{D\infty}$=0.4);

C_M = added-mass coefficient (C_M=0.5);

d = diameter of sediment;

d_n, d_s = forces working on dashpots;

e_n, e_s = forces working on springs;

e_{nmax}, e_{smax} = the upper limit of the compression force acting on the spring;
f_n, f_s = normal and tangential components of the force acting on the contacting plane between the i-th and j-th particles on the local coordinate system n-s;
g = gravitational acceleration;
h = water depth;
k_n, k_s = spring constants;
r_u, r_v = random numbers following to the standard Gauss distribution in x,y directions;
U = mean velocity component in x direction;
u, v = fluctuating components in x, y direction;
u_{pi}, v_{pi} = velocity of particles in x,y directions;
u_* = shear velocity;
$\sqrt{\overline{u^2}}$, $\sqrt{\overline{v^2}}$ = turbulent intensities in x,y directions;
x, y = streamwise and upward-vertical coordinates;
α_{ij} = contacting angle between the i-th and j-th particles;
γ = cross correlation coefficient of two series of the random numbers in the distribution of the flow turbulence;
$\Delta\xi_n$, $\Delta\xi_s$ = displacement of particle during the time Δt;
Δt = time step of the calculation;
η_n, η_s = damping coefficients;
ρ = density of fluid;
σ = density of sediment particle;
μ = coefficient of friction; *and*
ω_{pi} = angular velocity of the i-th particle.

(Received June 23, 1999 ; revised March 7, 2000)